PET Imaging of Osteosarcoma in Dogs Using a Fluorine-18-Labeled Monoclonal Antibody Fab Fragment

Rodney L. Page, Pradeep K. Garg, Sudha Garg, Gary E. Archer, Øyvind S. Bruland and Michael R. Zalutsky

College of Veterinary Medicine, North Carolina State University, Raleigh, Departments of Radiology and Pathology, Duke University Medical Center, Durham, North Carolina and Norske Radium Hospital, Oslo, Norway

Four dogs with histologically confirmed osteogenic sarcoma were studied with PET following intravenous injection of the ^{18}F-labeled Fab fragment of TP-3, a monoclonal antibody specific for human and canine osteosarcomas. **Methods:** The antibody fragment was labeled using the *N*-succinimidyl 8-[(4'-[^{18}F]fluorobenzyl)amino]suberate acylation agent. Blood clearance of activity was biphasic in all dogs but half-times were variable ($T_{1/2\beta}$ = 2–13 hr). Catabolism of labeled Fab was reflected by the decrease in protein-associated activity in serum from more than 90% at 1 min to 60%–80% at 4 hr. **Results:** PET images demonstrated increased accumulation of ^{18}F at the primary tumor site relative to normal contralateral bone in one dog as early as 15 min after injection. Biopsies obtained after euthanasia indicated higher uptake at the edges of the tumor as observed on the PET scans. Tumor uptake was 1–3 × 10^{-3}% injected dose/g, a level similar to that reported for other Fab fragments in human tumors. In the three dogs with metastatic disease, early PET images reflected activity in the blood pool but later uptake was observed in suspected metastatic sites. **Conclusions:** These results, although preliminary, suggest that PET imaging of ^{18}F-labeled antibody fragments is feasible and that dogs with spontaneous tumors could be a valuable model for preclinical research with radioimmunoconjugates.

Key Words: monoclonal antibody; PET; radioimmunoscintigraphy; dogs

J Nucl Med 1994; 35:1506–1513

Significant immunologic, physiologic and chemical impediments that limit selective tumor imaging and radioimmunotherapy with monoclonal antibodies (Mabs) have been identified. Some of these barriers include the anti-mouse antibody response, distribution limitations of macromolecules and radioconjugate degradation. Recent advances in recombinant antibody technology (chimeric antibodies), Mab radiolabeling chemistry and the development of strategies to improve Mab delivery to tumors suggest that progress toward overcoming some of these obstacles may be possible (*1,2*). However, systematic preclinical evaluation of technological refinements has been hindered by the absence of an animal model relevant to the human clinical setting.

Rodent xenograft models have been critical to the development of radiolabeled Mabs but extrapolation of data obtained from murine studies to humans must be done with caution. For example, in athymic mouse models, uptake of radioiodinated 81C6 Mab in subcutaneous glioma xenografts was 15%–25% of the injected dose (ID)/g (*3*) while in glioma patients, only 1–5 × 10^{-3}% ID/g tumor accumulation was observed (*4*). Concern also has been raised regarding the relevance of an immunodeficient rodent model for investigation of immune-based therapy in immunocompetent humans (*5*). In addition, dissimilarities in antibody biodistribution often occur in normal tissues because of the presence of antigen on normal humans but not murine tissues (*6*). An additional problem for therapeutic applications of labeled Mabs is the documented difference in radiation sensitivity of hematopoietic stem cells between rodents and humans (*7*).

Dogs may represent a more appropriate model for investigation of issues related to radioimmunotherapy for several reasons: (1) quantitative descriptions of radiopharmaceutical biodistribution to normal and tumor tissue can be more thorough (i.e., multiple samples can be obtained from most tissues); (2) canine bone marrow sensitivity to radiation is similar to humans (*7*); (3) techniques developed in normal dogs can be extended to clinical trials in dogs with spontaneously occurring neoplasia; and (4) dogs are large enough to undergo dynamic nuclear imaging studies using SPECT or PET to develop radiation dosimetry estimates.

One potential improvement in radioimmunoscintigraphy that might benefit from preclinical evaluation in dogs is the use of PET imaging. This modality is of interest because it offers the possibility of improving lesion detection and quantitation of both tumor and normal tissue uptake. We have developed methods for labeling Mab fragments with ^{18}F without adversely compromising their immunoreactivity (*8,9*). Although selective uptake of ^{18}F accumulation in subcutaneous human glioma xenografts could be demon-

Received Sept. 10, 1993; revision accepted Mar. 31, 1994.

For correspondence or reprints contact: R.L. Page, DVM, North Carolina State University College of Veterinary Medicine, 4700 Hillsborough St., Raleigh, NC 27606.

strated in a time frame compatible with the 2-hr half-life of this nuclide (*10,11*), the implications of these results to the imaging of human patients is not clear.

The current study was conducted in dogs with spontaneous primary and metastatic osteosarcomas to determine the feasibility of imaging tumors using ^{18}F-labeled Mab fragments. The Fab fragment of TP-3 was used because this Mab reacts with osteosarcomas of both canine and human origin (*12,13*), making these observations of potential relevance to the diagnosis of both patient populations. With regard to human patients, CT is generally used for the diagnosis of pulmonary metastases; however, in most cases, the surgeon will discover more lesions at thoracotomy than anticipated from the CT scan (*14*). Conversely, not all lesions detected on CT scan represent metastases (*15*). Thus, improving the detection of occult metastases is clearly needed and could lead to better individualization of therapy according to the extent of disease.

MATERIALS AND METHODS

Canine Patients

Four dogs with histologically proven osteogenic sarcoma were studied. Two dogs were imaged twice. All dogs were referred to the North Carolina State University College of Veterinary Medicine Oncology Service and informed consent was obtained from owners for these procedures. All procedures were approved by the NCSU Animal Care and Use Committee.

Immediately prior to the PET imaging studies, routine evaluation of the health status for each dog was conducted. This included complete blood count, serum biochemical panel, urinalysis and survey radiographs of the primary tumor, as well as any potential sites of metastasis in the thorax or abdomen. Additional diagnostic and staging procedures were conducted as indicated by the clinical condition of each dog. All dogs weighed approximately 25 kg.

Monoclonal Antibody

Murine Mab TP-3 is an IgG_{2b} derived following the immunization of mice with cells from a human osteosarcoma that had been serially passaged as a xenograft in athymic mice (*12*). This Mab reacts with an epitope on an 80-kD antigen that appears to be an osteoblastic differentiation marker (*16*). Mab TP-3 was purified from athymic mouse ascites by affinity chromatography on a Protein A-Sepharose column. Fab fragments were generated by papain digestion at a Mab-to-papain concentration ratio of 100:1 (w/w) and 10 m*M* of dithiothreotol. After 4 hr incubation at 37°C, the reaction was terminated by the addition of iodoacetamide (to a final concentration of 24 m*M*).

Labeling Procedure

A detailed description of the method for labeling Mab fragments with ^{18}F using the acylation agent *N*-succinimidyl 8-[(4'-[^{18}F]fluorobenzyl)amino]suberate (SFBS) has been described in a previous publication (*8*). Briefly, after converting aqueous [^{18}F]fluoride to tetrabutylammonium [^{18}F]fluoride, 4-[^{18}F]fluorobenzonitrile was prepared using a fluoro for nitro exchange reaction on 4-nitrobenzonitrile. Reduction to 4-[^{18}F]fluorobenzylamine was accomplished in quantitative yields using lithium aluminum hydride. Reaction of 4-[^{18}F]fluorobenzylamine with disuccinimidyl suberate at room temperature, followed by high-performance liquid chromatography purification of the crude reaction mixture, gave the required ^{18}F-labeled acylation agent, SFBS, in a 30%–35% decay-corrected overall yield.

The organic solvent containing the SFBS was evaporated under a gentle stream of nitrogen and reacted with 600–1000 μg (4 mg/ml) of TP-3 Fab in borate buffer (pH 8.5) at room temperature for 20 min. The reaction was terminated by adding 200 μl of 0.2 *M* glycine in 0.1 *M* borate buffer. The ^{18}F-labeled TP-3 fragment was isolated from small molecular weight impurities using a Sephadex G-25 column. Protein-associated radioactivity for purified ^{18}F-labeled TP-3 Fab, as determined by 20% trichloroacetic acid precipitation, was greater than 98% for all preparations.

Immunoreactivity of the ^{18}F-labeled TP-3 fragment was determined using the antigen-positive OHS human osteosarcoma cell line (*17*). Cells were grown in 100-mm petri dishes with Richter's Zinc Option media (Gibco, Grand Island, NY) supplemented with 10% fetal calf serum. Cells were removed with 0.02% EDTA in Dubelco's phosphate buffered saline (DPBS; Gibco), pelleted, washed once with DPBS and fixed with acetone at 0°C for 60 sec. The cells were pelleted (4×10^5 cells/tube) and resuspended in DPBS and stored at 4°C until needed. Between 2 and 10 ng of labeled Mab fragment was added in quadruplicate and incubated at 37°C for 3 hr. The cells were washed with PBS and then solubilized with 0.5 N NaOH and removed from the wells using cotton swabs. Each set of cotton swabs was counted along with input standards in an automated gamma-counter and the immunoreactive fraction was calculated (*18*).

PET Data Acquisition and Processing

Prior to each imaging session, the dogs were anesthetized intravenously using thiopental (12 mg/kg) and maintained on isoflorane inhalation anesthesia. Electrocardiographic and blood pressure monitoring were performed continuously during the procedure and 0.9% saline was administered intravenously during the procedure at 10 ml/kg/hr. A urinary catheter/collection system was maintained in all dogs. Dogs were in dorsal recumbency for all imaging.

The positron tomograph used on Dog 1 was an ECAT III (911-2A, CTI, Knoxville, TN) with a resolution of 8.6 mm (FWHM). The positron tomograph used on all other dogs was a GE 4096 PLUS (GE Medical Systems, Milwaukee, WI) with a resolution of 6.8 mm (FWHM). Prior to injection of the ^{18}F-labeled Mab fragment, a 10-min transmission scan was acquired using a ^{68}Ga/^{68}Ge source. Following intravenous injection of 1.0–11.8 mCi (1 mg) of ^{18}F-labeled TP-3 Fab, serial 20-min PET images (15 min for Dog 1) were obtained for 4 hr. All images on both scanners were reconstructed using calculated or geometric attenuation using a Hann 0.5 filter. In the first dog, regions of interest (ROIs) were drawn around the tumor and a corresponding area on the contralateral normal limb and the ratio of activity was calculated on a cpm/pixel basis. In dogs with metastatic disease, ROIs were drawn around suspected areas of tumor and activity levels were compared to ^{18}F dose standards of known activity level. All dogs except Dog 1 recovered uneventfully from the imaging procedure and had no adverse side effects.

Tissue and Blood Analyses

Immediately following the PET imaging session, Dog 1 was euthanized using a concentrated barbiturate solution and samples of tumor were obtained along the scanning plane. Samples were weighed and counted in an automated gamma counter and compared to injection standards to determine %ID/g uptake. With the exception of the first study on Dog 2, serial blood samples were

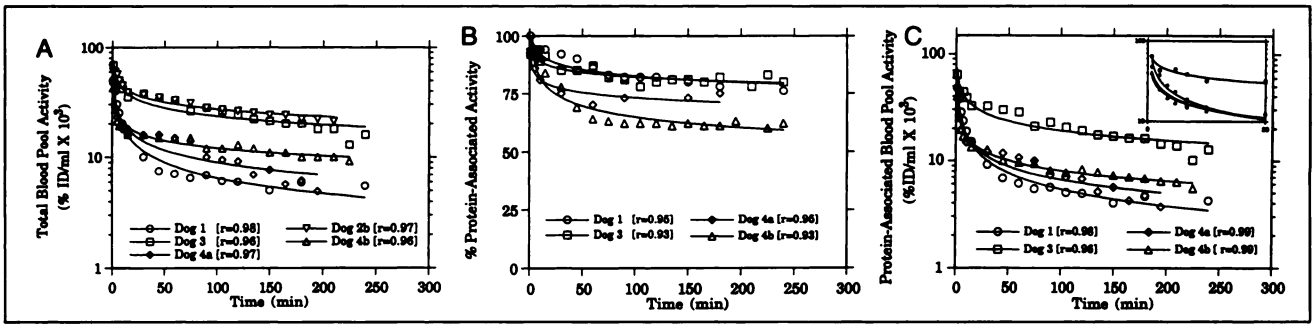

FIGURE 1. (A) Blood-activity elimination curves in dogs after a bolus injection of ^{18}F-labeled TP-3 Fab fragment. Study 4A and 4B were from the same dog injected approximately 1 mo apart (r-values represent correlation coefficients for logistic regression of data points). (B) Catabolism of protein-associated activity during study period for three dogs. Study 4A and 4B represent data from Dog 4 (r-values represent correlation coefficients from logistic regression of data points). (C) Elimination curves for the clearance of protein-associated ^{18}F activity from serum. Inset represents magnification of first 30 min after injection.

collected during the course of the imaging procedure. The samples were counted and the blood clearance half-times calculated using a computer program. Protein-associated activity in serial serum samples was also determined by precipitation with 20% trichloroacetic acid.

Nonparametric pharmacokinetic analyses were conducted for the plasma protein-associated activity data using statistical moment methods (*19*). Area under the concentration-activity curves (AUC) and area under the first moment curves (AUMC) were estimated using the trapezoid rule. Mean residence time (MRT) was computed as MRT = AUMC/AUC. Total body clearance (Cl_b) was expressed as Cl_b = D/AUC, where D = injected dose. Apparent volume of distribution at steady state (Vd_{ss}) was calculated as Vd_{ss} = (MRT)(Cl_b). Cl_b and Vd_{ss} were normalized to the body surface area of each dog in M^2. Elimination half-life ($T_{1/2}$) was determined by $T_{1/2}$ = (ln2)(MRT).

RESULTS

Mab Fragment Labeling

Overall yields for the labeling of the TP-3 Mab fragment were 2–3 mCi per 100 mCi of [^{18}F]fluoride in a total synthesis time of 65–80 min. With the exception of the last study, the coupling efficiency of SFBS to TP-3 Fab was 15%–20%. As a result, in the first five studies, dogs received 1–4 mCi of ^{18}F-labeled Mab fragment and in the last study, a dose of 11.8 mCi was used. The specific activity of the preparations ranged from 1–11.8 mCi/mg. The immunoreactive fraction for TP-3 Mab fragment after labeling with ^{18}F was 50%–61%.

Pharmacokinetics

A total of six studies were performed on four dogs with primary and metastatic osteosarcoma. With the exception of the first study on Dog 2, 15–20 blood samples were obtained from 1 min to 4 hr after injection of ^{18}F-labeled TP-3 Fab in order to determine blood clearance half-times (Fig. 1A). In all cases, a biphasic washout of ^{18}F activity from blood was observed. The first component (distribution) half-time was rapid, ranging from 3 to 22 min (Table 1). Except for Dog 2, the distribution phase accounted for the majority of the ^{18}F clearance from serum. The elimination phase half-time ranged from 2.0 to 13.1 hr.

The protein-associated fraction of ^{18}F activity in the serum was determined by trichloroacetic acid (TCA) precipitability in order to monitor the catabolism of label from the Mab fragment. Prior to injection, greater than 98% of the ^{18}F activity was TCA precipitable. As shown in Figure 1B, the fraction of protein-associated activity decreased during the first 60 min after injection and then remained relatively constant thereafter. These plateau levels ranged from about 75% to 85%. The decrease in TCA precipitable activity in the serum exhibited biexponential behavior (Fig. 1C).

The pharmacokinetic parameters calculated for the protein-associated blood pool ^{18}F activity are summarized in Table 2. Dog 2 was omitted from these analyses because blood samples were not collected in the first study and the protein-associated activity was not measured during the second study. Dog 3 had reduced clearance and volume of distribution relative to the other dogs and this accounted for a substantial increase in the AUC for this dog. In Dog 4, there was good agreement in the pharmacokinetic parameters calculated for the first and the second injections.

Dog 1

Dog 1 was an 8-yr-old, neutered male Great Pyrenees with a 4–5-cm osteosarcoma on the left distal radius

TABLE 1
Blood Clearance of ^{18}F Activity in Dogs Injected with ^{18}F-Labeled TP-3 Fab Fragment

Dog	Distribution half-time $T_{1/2\alpha}$ (min)	Elimination half-time $T_{1/2\beta}$ (h)	% Slow component
1	8	13.1	15
2A	ND*	ND	ND
2B	22	2.5	68
3	7	2.3	35
4A	3	2.0	29
4B	4	4.6	24

*ND = not done.

TABLE 2
Pharmacokinetic Parameters for the Protein-Associated Activity in Dogs after an Intravenous Bolus of ^{18}F-Labeled TP3 Fab Fragment

Parameter	Dog 1	Dog 3	Dog 4A	Dog 4B
AUC (%ID-min/ml)	1.6	5.1	1.7	2.0
Cl_b (ml/min/M^2)	73.5	23.0	69.6	58.0
Vd_{ss} (L/M^2)	6.3	2.2	5.0	5.4
$T_{1/2}$ (min)	59.9	66.5	50.0	64.6

(Fig. 2A). The dog had not undergone chemotherapy or other treatment prior to PET imaging. Imaging was performed with the forelimbs parallel to the torso at three bed positions (three planes per position). Even at early time points, increased accumulation was observed in the most distal and proximal planes—but not middle planes—of the tumor-bearing limb. Figure 2C illustrates a PET image of the most proximal plane obtained 105 min after injection of the ^{18}F-labeled TP-3 Fab fragment. The ratio of activity in tumor, compared to contralateral normal bone, is presented in Figure 2D. An uptake ratio near unity was seen in the middle planes while both the most proximal and distal planes indicated preferential accumulation of tracer in the tumor *versus* normal limb.

Four hours after injection of the labeled Mab fragment, the dog was euthanized and trephine biopsies were obtained along the long-axis of the tumor, perpendicular to the image plane. The overall pattern of uptake of radioactivity in the tumor samples was similar to that seen in the PET images. As shown in Figure 2E, ^{18}F uptake was 1.6 × 10^{-3}% ID/g in the most proximal sample, decreased to 0.8–1.3 × 10^{-3}% ID/g in the middle samples, and increased to 2.7 × 10^{-3}% ID/g in the most distal sample.

Dog 2

Dog 2 was an 8-yr-old female mixed breed. The primary osteosarcoma on the humerus had been amputated and pulmonary and subcutaneous metastases were present at the time of PET imaging. The dog was imaged twice with the second session occurring 3 wk later, and 1 wk after the initiation of Cisplatin therapy (Platinol, Bristol Laboratories, Evanston, IL). Figure 3A from the first study illustrates transaxial PET images of the thorax obtained between 60 and 200 min after injection of 3.8 mCi of ^{18}F-labeled TP-3 Fab. Earlier images reflected high levels of activity in the blood pool but on these later images, increased uptake of activity in a focal lesion in the left lung was seen. The location of this intrathoracic uptake was consistent with a solitary metastatic nodule seen on survey radiographs. When this dog was imaged 3 wk later after the initiation of chemotherapy, decreased accumulation in the nodule was noted although no difference in nodule size was seen in radiographs.

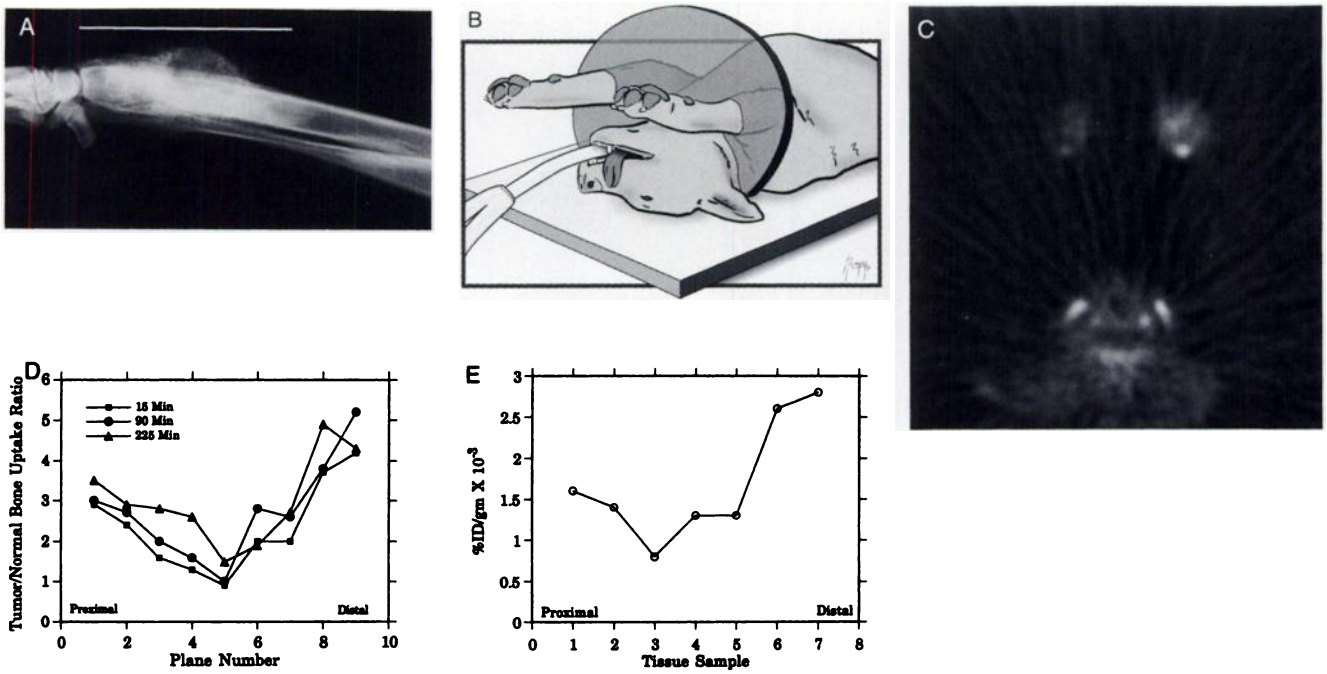

FIGURE 2. (A) Lateral radiograph of distal radius from Dog 1 illustrates primary osteosarcoma. Bar indicates region imaged with PET after injection of ^{18}F-labeled TP-3 Fab fragment and subsequently sampled. (B) Schematic drawing of dog in dorsal recumbency indicating plane of transection depicted in Figure 2C. (C) PET image from most proximal plane 105 min after injection. Dog in dorsal recumbency with tumor-bearing leg in upper right, normal leg in upper left and neck region in lower half of the image. Hot regions in neck presumed to correspond to jugular vein activity. (D) Tumor-to-normal bone uptake ratio as a function of imaging plane during PET. The uptake ratio was calculated by comparing activity in tumor plane relative to normal bone activity in the opposite normal front limb that was imaged simultaneously. (E) Percent of injected activity/g of tissue samples obtained from regions corresponding to imaging planes identified in Figure 2C.

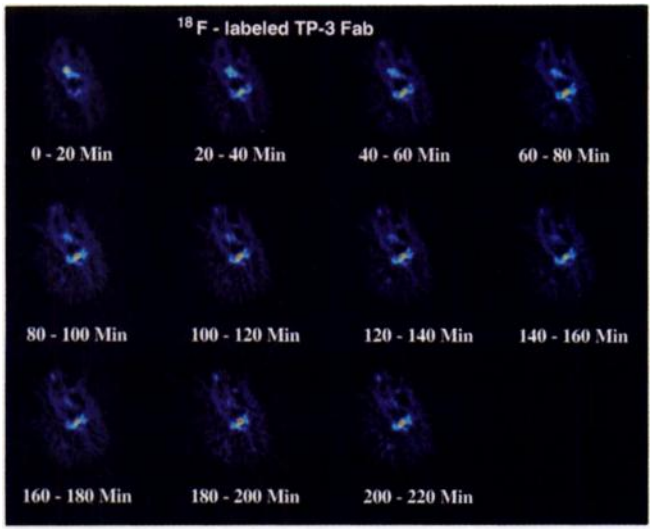

FIGURE 3. Transaxial PET images over the 4-hr study interval from Dog 2 demonstrating accumulation of activity in metastatic nodule after washout of blood-pool activity.

Dog 3

Dog 3 was an 8-yr-old male golden retriever that had undergone amputation to remove an osteosarcoma on the left distal radius. Thoracic radiographs indicated the presence of a 5–8-cm diameter extrapleural mass associated with the seventh rib. As shown in Figure 4, with time, a gradual washout of activity from the blood pool was noted with increasing accumulation seen in a site corresponding to the rib metastasis. The activity from the PET images in an ROI set over the center of this lesion increased from 23 nCi/cc at 30 min to 45 nCi/cc at 150 min and remained relatively constant at this level until the end of the 4-hr

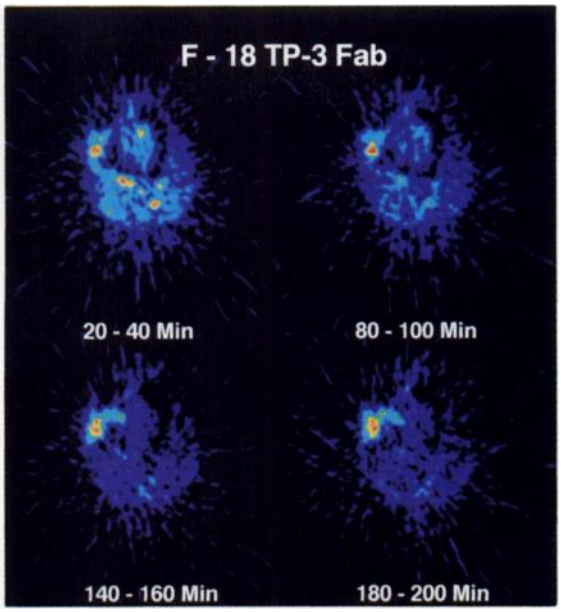

FIGURE 4. Selected transaxial PET images during the study interval from Dog 3 demonstrating accumulation of activity in a metastatic nodule associated with right anterior pleura.

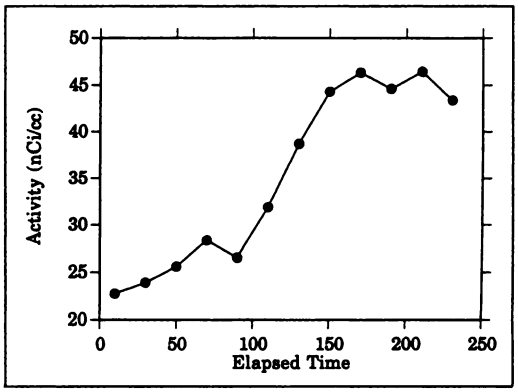

FIGURE 5. Activity as a function of time in the region of interest set over the center of the lesion indicated in Figure 4 in Dog 3.

study (Fig. 5). Assuming unit density for tumor, these values correspond to 1.5 and 3.0 × 10^{-3}% ID/g, respectively.

Dog 4

Dog 4 was an 18-mo-old German shepherd that had an osteosarcoma on the tibia that had been removed by amputation. PET imaging of the thorax was performed twice, 3 wk apart (Study 4a and 4b). In both studies, a large photopenic region in the right lung with increased uptake on the periphery was noted (Fig. 6). An autopsy performed shortly after the second study revealed a large, avascular necrotic mass in the right lung.

DISCUSSION

Radioimmunotherapy treatment planning would be greatly facilitated if more accurate tumor and normal tissue

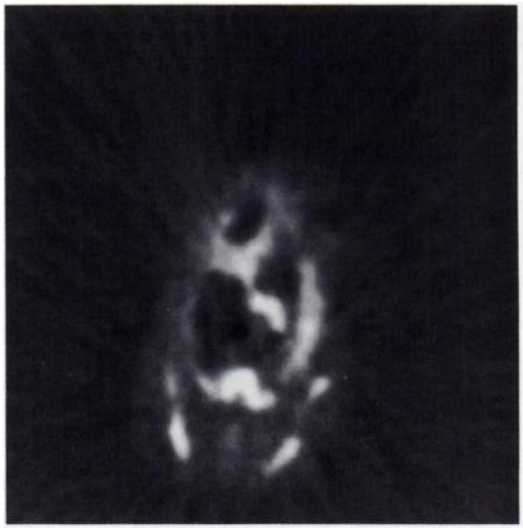

FIGURE 6. Transaxial PET image from Dog 4 indicating a large peripherally enhanced region which surrounds a photophenic region in the right anterior lung. Regions of enhanced uptake relate to persistent blood pool activity. These include heart and active bone marrow. Ultrasonographic evaluation and subsequent autopsy confirmed this mass to be a neoplastic nodule with a necrotic, avascular region.

dosimetry was available. A recent review has underscored the need for performing SPECT to quantitate tissue activity levels after the administration of radiolabeled Mabs (*20*). For example, SPECT has been used to investigate the relationship between Mab protein dose and normal tissue and tumor dosimetry (*21*). Because of the imaging advantages (sensitivity, contrast resolution) and quantitative capabilities of PET, Mabs labeled with positron-emitting nuclides might be an even more attractive approach not only for dosimetry estimation but also because of its potential for improving lesion detection, particularly at early time points.

To date, clinical studies combining PET and Mabs have been quite limited. Larson et al. (*22*) used PET imaging of an ^{124}I-labeled Mab to determine dosimetry in a child with neuroblastoma. The detection of lymph node metastases confirmed at surgery using a ^{64}Cu-labeled Mab that were not detected by CT has also been reported (*23*). Although these preliminary results are encouraging, the potential clinical utility of ^{124}I- and ^{64}Cu- may be limited because of the lack of availability of these nuclides.

The current study was performed to explore the feasibility of using Mab fragments labeled with ^{18}F for the detection of tumors using PET. This nuclide was selected because it has the longest half-life of the routinely available positron emitters. Nonetheless, serious concerns exist about whether tumor targeting of a labeled Mab fragment can be achieved at imaging times that are compatible with the half-life of ^{18}F. Our initial attempts to address this issue were performed in an athymic mouse model with ^{18}F-labeled Mel-14 F(ab')$_2$ fragments (*10,11*). These studies demonstrated selective and specific uptake in D-54 MG human glioma xenografts 4–6 hr after injection. In addition, these experiments indicated nearly identical uptake of co-administered radioiodinated Mel-14 F(ab')$_2$ in tumor and most normal tissues. While it is not certain which therapeutic nuclide would be best used in tandem with ^{18}F (the 7.2-hr half-life radiohalogen ^{211}At is a possibility), it will be critical to document equivalent pharmacokinetic behavior of the two antibody labels after in vivo administration.

The results obtained with ^{18}F-labeled Mab fragments in athymic mice bearing human tumor xenografts are encouraging; however, extrapolation of murine tissue distribution data, particularly with regard to the kinetics of tumor localization, must be done with extreme caution. For this reason, this study extended our investigation of the feasibility of imaging tumors using PET and ^{18}F-labeled Mabs to a larger and more relevant species.

The use of dogs with tumors as a precursor to human studies with diagnostic and therapeutic radiopharmaceuticals offers several advantages. Cancer in dogs develops spontaneously as a result of similar environmental and genetic factors that account for human cancer, and occur in an outbred, older population where physiological and genetic diversity is similar to humans (*24*). Many tumor types that arise in dogs are similar biologically and epidemiologically to human tumors (melanoma, non-Hodgkins lymphoma, osteosarcoma) and have been previously used as valuable models (*25–28*). Clinical trials in dogs can be rigorously conducted with the same quality control as human studies, however, endpoints can be evaluated more rapidly because of the contracted life span of dogs. In addition, a high autopsy rate (>80%) is commonly achieved in clinical studies involving pet animals. Thus, while canine clinical studies will not replace the need for murine models, they may compliment and extend the preclinical evaluation of new diagnostic and treatment strategies.

Because of our long-term goal of extending this approach to humans, a Mab was selected that exhibited reactivity with both a canine and human tumor. Mabs TP-3 and TP-1 react with different epitopes of an antigen present on osteosarcomas from both species (*12,13*). Imaging of lung metastases in humans using radiolabeled TP-1 F(ab')$_2$ has been described in a preliminary report (*29*). Although imaging of canine osteosarcoma using radioiodinated TP-1 F(ab')$_2$ has been reported (*30*), tumor-to-normal tissue ratios were only 1.5-2.5. Since immunohistochemical analysis indicated that TP-3 stained virtually all canine osteosarcoma cells while TP-1 stained fewer cells with less intensity (*13*), we selected TP-3 for use in this study.

In most cases, yields for coupling SFBS to TP-3 Fab were lower than encountered with other Mab fragments (*8,11*). Parallel labelings of TP-3 Fab using *N*-succinimidyl 3-[^{125}I]iodobenzoate, which also reacts with lysines, gave three- to fivefold higher coupling efficiencies than seen with SFBS. While the reason for the reduced yield for coupling SFBS to TP-3 Fab is not known, we can only speculate that the 8-carbon spacer between the active ester and the aryl fluoride in SFBS could lower yields with Mabs where steric access to lysine residues is a problem. The immunoreactive fraction for ^{18}F-labeled TP-3 Fab was 50%–61%, a range comparable to that seen with other Mab fragments labeled using SFBS (*8,11*). These results are also consistent with those reported for intact TP-3 IgG following radioiodination using the iodogen method (*31*).

The Fab fragment of TP-3 Mab was selected for evaluation because of the more rapid blood clearance of this molecule compared to intact IgG and F(ab')$_2$ fragments (*32*). Rapid clearance of ^{18}F activity from the blood pool was seen, an observation critical to the use of ^{18}F-labeled Mab fragments for imaging. With the exception of one study, more than 50% of the activity cleared from the blood pool in less than 30 min. The elimination phase half-times observed were between 2.0 and 4.6 hr, except for Dog 1, where a significantly longer half-time was seen. It should be noted that this was the only dog that had not undergone an amputation to remove the primary tumor prior to the study.

The pharmacological handling of a radiopharmaceutical may be described by several methods. In this study, the distribution and elimination phase half-times were calculated for total activity in the blood pool to describe the general handling of the isotope for imaging purposes. A

more complete description of the protein-associated ^{18}F activity, presumably representing Fab and its protein catabolites, was conducted using nonparametric pharmacokinetic analysis.

The AUC is classically considered a better indicator of systemic exposure than the administered dose of drug and dose escalation studies since increments of AUC are generally more efficient than escalation schemes based on some factor of dose (*33*). Correlation of toxicity to AUC may be similarly useful in future radioimmunotherapy Phase I studies since blood sample analysis is rapid for radiopharmaceuticals compared to drug analysis. Dog 3 had a substantially increased AUC compared to the other dogs due to reduced clearance and distribution. Interestingly, the systemic handling (Cl_b, Vd_{ss} and $T_{1/2}$) of activity was similar in the two studies performed on Dog 4. This might have been unexpected because of the potential for an antimurine immune response affecting Mab clearance in the second study. Likewise, tumor progression between treatments could have increased the tumor compartment and subsequently increased the volume of distribution. If Mab pharmacokinetic data in the dogs are found to be relevant to humans, then more thorough investigations of this type may help optimize strategies for Mab administration.

The variation in clearance between dogs is likely a result of multiple factors. Heterogeneity in nonspecific antibody binding and catabolism of the immunoconjugate may result in variable serum activity. With regard to catabolism of label, a biphasic and variable decline in protein-associated ^{18}F activity in the serum was seen in all dogs. The degree of loss in TCA-precipitable activity from TP-3 Fab over this time period was similar to that reported for other Fab fragments (*34*). All dogs in this study had normal hepatic and renal function as determined by serum biochemical assay; however, subclinical alterations in physiologic function due to age, nutritional status, tumor burden or concurrent medication may have influenced elimination of TP-3 Fab. Such factors also exist in humans undergoing clinical study.

One parameter for which murine xenograft studies are least predictive of clinical behavior is the magnitude of labeled Mab uptake in tumor. In general, the percent uptake per gram of tumor seen in xenografts has been at least three orders of magnitude less than that seen in patients (*6*). Although no data using TP-3 Fab in patients are available, biopsy studies performed in patients injected with other Fab fragments indicate tumor uptake of the order of 10^{-3}% ID/g (*6*). In the one dog from which biopsies of its primary osteosarcoma could be obtained, and in the dog in which activity levels in a rib metastasis were quantitated by PET, tumor levels of 1–3 × 10^{-3}% ID/g were seen. While these must be considered only anecdotal observations, they suggest that the tumor level of a labeled Mab fragment seen in spontaneous tumors in the dog may be predictive of what will be seen in a human clinical study. If confirmed, this finding supports the utility and relevance of this model for preclinical evaluation of labeled Mabs.

The key observation of the current study was that both primary and metastatic osteosarcomas could be imaged using an ^{18}F-labeled Fab fragment using PET. In the one dog with primary osteosarcoma, increased accumulation was noted in PET images as early as 15 min after injection. Higher activity levels were seen in image planes corresponding to peripheral tumor regions and a similar trend was observed in a series of tumor biopsies obtained immediately after imaging. While these results are encouraging, it should be noted that the location of the lesion in the limb would tend to minimize the interfering effect of radioactivity in the blood pool on tumor imaging. Of greater relevance to most human clinical applications are the studies performed in dogs with metastatic disease. Increased uptake in rib and pulmonary metastases was observed in regions corresponding to suspected lesion sites in all animals. As expected, in the dog with a large necrotic mass, uptake of labeled Mab was confined to peripheral regions.

In summary, uptake of ^{18}F-labeled TP-3 Fab fragment in primary and metastatic osteosarcoma in dogs could be demonstrated by PET imaging in a time frame compatible with the short half-life of this nuclide. The level of tumor accumulation was similar to that reported in patients with other labeled Fab fragments, suggesting the potential utility of dogs with spontaneous tumors as a model for the preclinical evaluation of labeled Mabs. While preliminary in nature, these results suggest that it may be feasible to image tumors in patients using ^{18}F-labeled Mab fragments and PET.

ACKNOWLEDGMENTS

The authors thank Sharon Hamblen and Thomas Hawk for help with the imaging studies and Sandra Gatling for assistance in the preparation of this manuscript. This work was supported in part by Department of Energy grant DE-FG05-89ER60789.

REFERENCES

1. Bast RC Jr, Zalutsky MR, Frankel AE. Monoclonal serotherapy. In: Holland JF, ed. *Cancer medicine*, third edition. Philadelphia: Lea and Febiger; 1993:968–982.
2. Fritzberg AR, Berninger RW, Hadley SW, Wester DW. Approaches to radiolabeling of antibodies for diagnosis and therapy of cancer. *Pharmaceutical Res* 1988;5:325–334.
3. Zalutsky MR, Noska MA, Colapinto EV, Garg PK, Bigner DD. Enhanced tumor localization and *in vivo* stability of a monoclonal antibody radioiodinated using *N*-succinimidyl 3-(tri-*n*-butylstannyl)benzoate. *Cancer Res* 1989;49:5543–5549.
4. Zalutsky MR, Moseley RP, Coakham HB, Coleman RE, Bigner DD. Pharmacokinetics and tumor localization of ^{131}I-labeled anti-tenascin monoclonal antibody 81C6 in patients with gliomas and other intracranial malignancies. *Cancer Res* 1989;49:2807–2813.
5. Sands H. Experimental studies of radioimmunodetection of cancer: an overview. *Cancer Res* 1990;50(suppl):809s–813s.
6. Carrasquillo JA. Radioimmunoscintigraphy with polyclonal or monoclonal antibodies. In: Zalutsky MR, ed. *Antibodies in radiodiagnosis and therapy*. Boca Raton, FL: CRC Press; 1989:169–198.
7. Vriesendorp HM, Quadri SM, Stinson RL, et al. Selection of reagents for human radioimmunotherapy. *Int J Radiat Oncol* 1991;22:37–45.
8. Garg PK, Garg S, Zalutsky MR. Fluorine-18 labeling of monoclonal antibodies and fragments with preservation of immunoreactivity. *Bioconjugate Chem* 1991;2:44–49.

9. Vaidyanathan G, Zalutsky MR. Labeling proteins with fluorine-18 using *N*-succinimidyl 4-[^{18}F]fluorobenzoate. *Nucl Med Biol* 1992;19:275–281.
10. Vaidyanathan G, Bigner DD, Zalutsky MR. Fluorine-18-labeled monoclonal antibody fragments: a potential approach for combining radioimmunoscintigraphy and positron emission tomography. *J Nucl Med* 1992;33:1535–1541.
11. Garg PK, Garg S, Bigner DD, Zalutsky MR. Localization of fluorine-18-labeled Mel-14 monoclonal antibody F(ab')$_2$ fragment in a subcutaneous xenograft model. *Cancer Res* 1992;52:5054–5060.
12. Bruland Ø, Fodstad Ø, Funderud S, Pihl A. New monoclonal antibodies specific for human sarcomas. *Int J Cancer* 1986;38:27–31.
13. Haines DM, Bruland ØS. Immunohistochemical detection of osteosarcoma-associated antigen in canine osteosarcoma. *Anticancer Res* 1989;9:903–908.
14. Creagan E, Frytak S, Pairolero P, et al. Surgically proven pulmonary metastases not demonstrated by computed chest tomography. *Cancer Treat Rep* 1978;62:1404–1405.
15. Santrach P, Askin F, Wells R, et al. Nodular form of bleomycin-related injury with osteosarcoma. *Cancer* 1989;64:806–811.
16. Bruland ØS, Fodstad Ø, Stenwig AE, Pihl A. Expression and characteristics of a novel human osteosarcoma-associated cell surface antigen. *Cancer Res* 1988;48:5302–5309.
17. Fodstad Ø, Brøgger A, Bruland Ø, Solheim ØP, Nesland JM, Pihl A. Characteristics of a cell line established from a patient with multiple osteosarcoma, appearing 13 yr after treatment for bilateral retinoblastoma. *Int J Cancer* 1986;38:33–40.
18. Lindmo T, Boven E, Cuttitta F, Fedorko J, Bunn Jr PA. Determination of the immunoreactive fraction of radiolabeled monoclonal antibodies by linear extrapolation to binding at infinite antigen excess. *J Immunol Meth* 1984;72:77–89.
19. Gibaldi M, Perrier D. *Pharmacokinetics*, second edition. New York: Marcel Dekker; 1982:409–417.
20. Leichner PK, Koral KF, Jaszczak RJ, Green AJ, Chen GTY, Roeske JC. An overview of imaging techniques and physical aspects of treatment planning in radioimmunotherapy. *Med Phys* 1993;20:569–577.
21. Schold Jr SC, Zalutsky MR, Coleman RE, et al. Distribution and dosimetry of ^{123}I-labeled monoclonal antibody 81C6 in patients with anaplastic glioma. *Invest Radiol* 1993;28:488–496.
22. Larson ST, Pentlow KS, Volkow ND, et al. PET scanning of iodine-124-3F9 as an approach to tumor dosimetry during treatment planning for radioimmunotherapy in a child with neuroblastoma. *J Nucl Med* 1992;33:2020–2023.
23. Philpott GW, Schwarz SW, Anderson CJ, et al. Initial clinical study of Cu-64-labeled anticolon-carcinoma monoclonal antibody (Mab 1A3) in colorectal cancer [Abstract]. *J Nucl Med* 34:81–82P.
24. MacEwan EG. Spontaneous tumors in dogs and cats: models for the study of cancer biology and treatment. *Cancer Metast Rev* 1993;9:125–136.
25. MacEwen EG, Kurzman ID, Rosenthal RC, et al. Therapy for osteosarcoma in dogs with intravenous injection of liposome-encapsulated muramyl tripeptide. *J Natl Cancer Inst* 1989;81:935–938.
26. McChesney-Gillette S, Dewhirst MW, Gillette EL, et al. Response of canine soft tissue sarcomas to radiation or radiation plus hyperthermia: a randomized phase II study. *Int J Hyperther* 1992;8:309–320.
27. Page RL, Macy DW, Ogilvie GK, et al. Phase III evaluation of doxorubicin and whole-body hyperthermia in dogs with lymphoma. *Int J Hyperther* 1992;8:187–198.
28. Thrall DE, Dewhirst MW, Page RL, Samulski TV, McLeod DA, Oleson JR. A comparison of temperatures in canine solid tumours during local and whole-body hyperthermia administered alone and simultaneously. *Int J Hyperther* 1990;6:305–317.
29. Bruland Ø. Radio-immuno-targeting. *Farmakoterapi* 1991;47:1–16.
30. Haines DM, Bruland ØS, Matte G, Wilkinson AA, Meric SM, Fowler JD. Immunoscintigraphic detection of primary and metastatic canine osteosarcoma with F(ab')$_2$ fragments of osteosarcoma-associated monoclonal antibody TP-1. *Anti Cancer Res* 1992;12:2151–2157.
31. Bruland Ø, Fodstad Ø, Skretting A, Pihl A. Selective localisation of two radiolabelled anti-sarcoma monoclonal antibodies in human osteosarcoma xenografts. *Br J Cancer* 1987;56:21–25.
32. Zalutsky MR, Colcher D, Kaplan WD, Kufe DW. Radioiodinated B6.2 monoclonal antibody: further characterization of a potential radiopharmaceutical for the identification of breast tumors. *Int J Nucl Med Biol* 1985; 12:227–233.
33. Belani CP, Egorin MJ, Abrams JS, et al. A novel pharmacokinetically based approach to dose optimization of carboplatin when used in combination with etoposide. *J Clin Oncol* 1989;7:1896–1902.
34. Holton OD III, Black CDV, Parker RJ, et al. Biodistribution of monoclonal IgG1, F(ab')$_2$ and Fab' in mice after intravenous injection. *J Immunol* 1987;139:3041–3049.